IJSES
Volume 9, Issue 9, pp. 128-134, 2025.
International Journal of Scientific Engineering and Science
ISSN (Online): 2456-7361

The Nano Structural and Electrical Properties of Tin and Chromium Nitride Using UV-VIS spectrophotometer Techniques

Abobakr Abdourhaman Mohammed Salem[1], Sawsan Ahmed Elhouri Ahmed[2]
[1]Ph.D. Student - Khartoum-Sudan
[2]University of Bahri- College of Applied & Industrial Sciences
Department of Physics - Khartoum -Sudan

Abstract— *The subject of this the work is Chromium nitride compound and tin metal, those attracted the interest of researchers. Transition-metal nitrides (TMN) have a great technological importance due to its interesting physical properties such as extreme hardness, high melting temperature, high reflectivity, corrosion resistance, abrasive resistance, diffusion resistance, good stability at high temperatures, and good electrical and optical properties, etc., which makes them suitable for many important technological applications. These compounds used in engineering technology fields, such as metallurgy, electronic industries, high-temperature structural ceramics, microelectronic devices, industrial catalysts and in composites with other materials, which can improve their properties and even reveal new applications. In this work a quantity of chromium compound and tin metal were ground in mortar. Samples prepared and measurements were at room temperature. All samples were analyzed before and after grinding by using UV-visible Spectrophotometer. Also, this work was undertaken to investigated from effect of mechanical treatment on properties of the prepared samples, the possibility of obtaining new elements for the fabrication of solar cells, or their use in electronic devices.*

I. Introduction

Analysing the reactivity of transitional metal nitrides, researchers concluded [1,2,3] that nitrides can be produced by the direct action of Nitrogen (N) on the metal when the small N atoms, which satisfy the empirical Hagg rule of the 0.59 ratio between non-metal/metal atom radii [3], will occupy the octahedral spaces in the body-cantered cubic (BCC) Chromium (Cr) lattice and that the formed interstitial compound is influenced by the electrons in the metal's outer shell [1,2]. As such, having five electrons in the three-dimensional shell, Cr will form two nitrides: Chromium nitride (CrN) and Dichromium nitride (Cr_2N). Most of the characteristics of the base metal are retained by the resultant alloy. Furthermore, the existence of N atoms in the Cr lattice causes the production of metal-nonmetal bonds, and the connection is partially ionic because of the The variation in electronegativity between the two elements [4,5]. The resulting CrN has a higher melting point than the base metal, increased hardness, and retains the chemical stability of the base metal [6]. CrN coatings are widely used to protect surfaces from mechanical and chemical influences, and there are numerous publications detailing their characteristics, notably in tribological applications. where, due to specific criteria, hard metal coatings with low chemical reactivity are required [7,8]. CrN was proven as a great option for protective coating applications due to its hardness, low coefficient of friction and great corrosion resistance [9,10,]. Moreover, CrN exhibits good heat resistance [9,10] and great thermal stability [9,10]. These exceptional properties recommend CrN as a good candidate for microelectronics applications [10], especially in the domain of protection against corrosion, oxidation, and heat [10]. A remarkable property of CrN thin films is the tunability of resistivity with the orientation of crystallites [8], which opens a large palette of electrical applications of CrN. Supercapacitor applications represent another research area in which massive progress has been made in the last few years [9,10]. Because of their large specific capacitance and cycle stability, metal nitrides have significant promise as supercapacitor electrode materials. In the Ref. [9] the authors prepared CrN thin films by direct current magnetron (DC) sputtering on polished Si wafers. They found that electrochemical performance can be easily tuned by varying the deposition conditions. Depositing CrN thin films with thicknesses of tens of nanometres on silicon can be very useful for covering photovoltaic cells [10].

II. Material & Method

UV-VIS spectrophotometer

Electronic absorption or UV-visible analysis is one of the most basic optical techniques, and yet the most useful for study the optical and electronic properties of nanomaterials. In this work used SPUV-26, UV/VIS Double beam spectrophotometer wavelength range 190~1100 nm, manufactured in Germany shown in figure (1). The specifications of the device used are shown in the table (1).

TABLE 1: Specifications SPUV-26, UV/VIS Double beam spectrophotometer.

Model	SPUV-26
Wavelength Range	190-1100nm
Spectral Bandwidth	2nm (5nm, 4nm, 1nm optional)
Detector	Silicon photodiode
Power	AC:220V, 50/60Hz, 180W
Serial nu	111311

UV-VIS Spectrophotometer Results of All Samples

After we made the (Cr_2N and Sn-Tin) samples before and after grinding where Nanomaterial's are presented, used SPUV-26, UV/VIS spectrophotometer wavelength range 190~1100

International Journal of Scientific Engineering and Science
Volume 9, Issue 9, pp. 128-134, 2025.
ISSN (Online): 2456-7361

nm to evaluate some optical properties like (absorbance, transition, reflection, absorption coefficient, extinction coefficient, refractive index) and some optical constant like (optical energy band gap, rail and imagery dialectical constant) and some electrical properties.

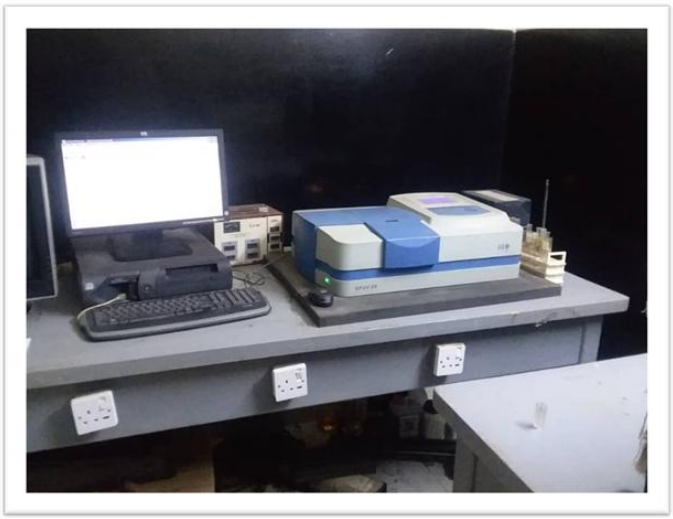

Figure 1: SPUV-26, UV/VIS Double Beam Spectrophotometer

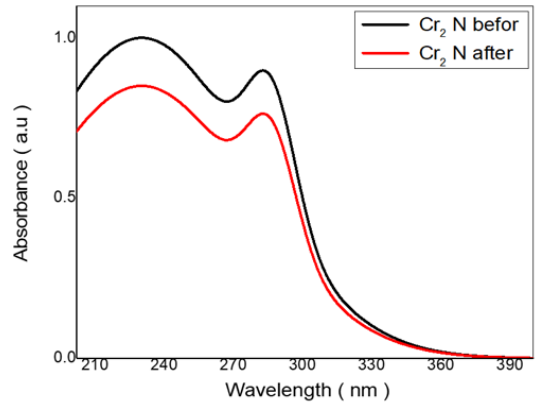

Figure 1: Relation Between Absorbance And Wavelengths Of Cr_2N Samples

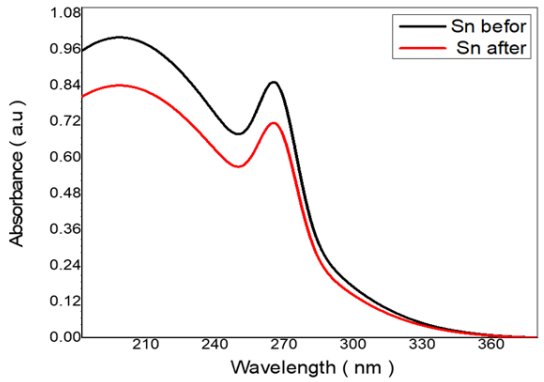

Figure 2: Relation Between Absorbance And Wavelengths Of Sn – Tin Samples

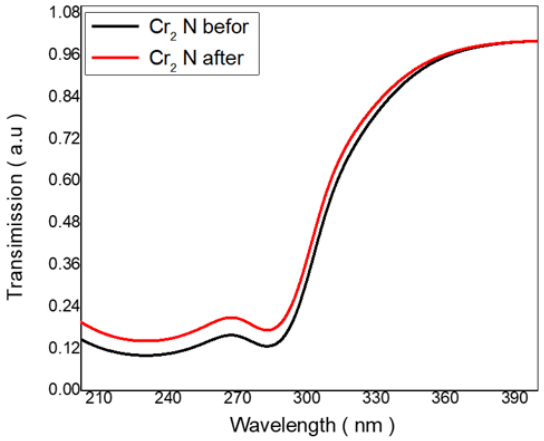

Figure 3: Relation Between Transimission and Wavelengths of Cr_2 N Samples

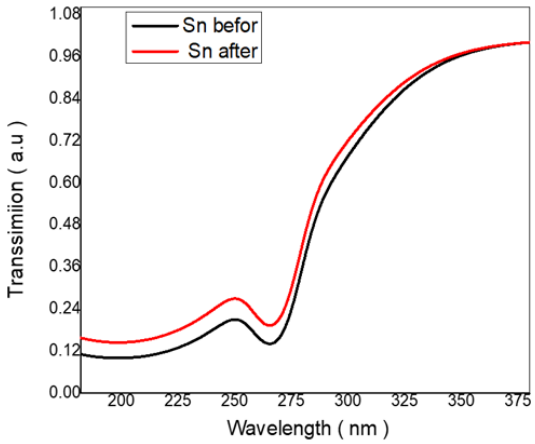

Figure 4: Relation Between Transimission and Wavelengths of Sn-Tin Samples

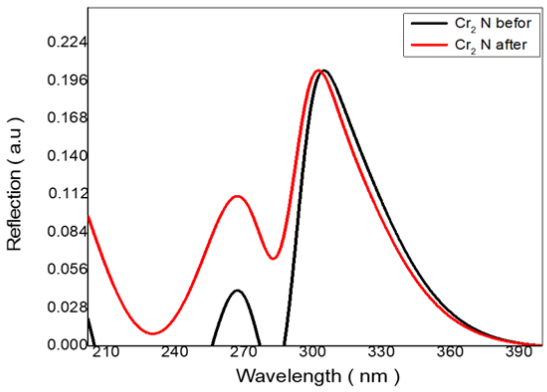

Figure 5: Relation Between Reflection and Wavelengths of Cr_2N Samples

International Journal of Scientific Engineering and Science
Volume 9, Issue 9, pp. 128-134, 2025. ISSN (Online): 2456-7361

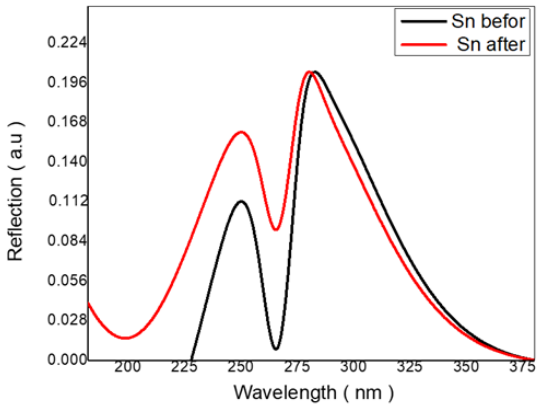

Figure 6: Relation Between Reflection and Wavelengths of Sn - Tin Samples

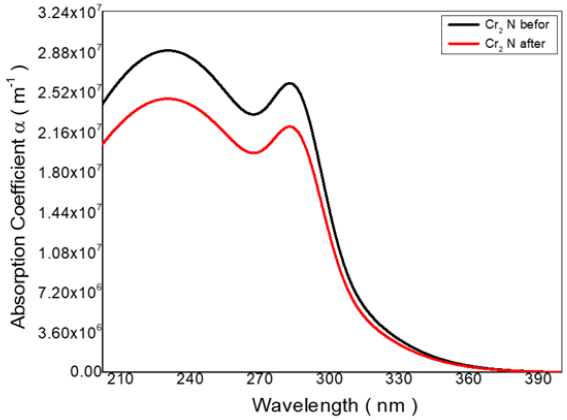

Figure 7: Relation Between Absorption Coefficient and Wavelengths of Cr_2N Samples

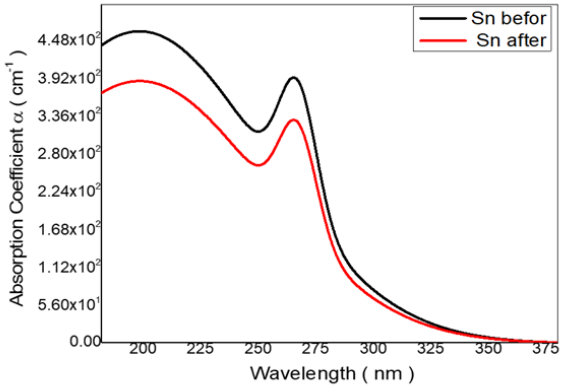

Figure 8: Relation Between Absorption Coefficient And Wavelengths Of Sn-Tin Samples

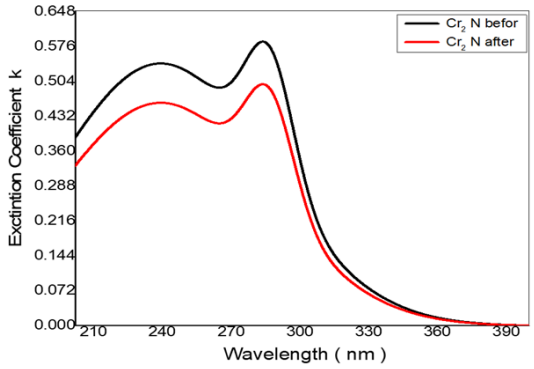

Figure 9: Relation Between Exctintion Coefficient and Wavelengths of Cr_2N Samples

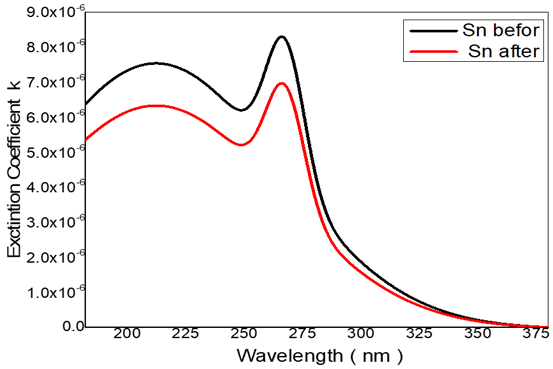

Figure 10: Relation Between Exctintion Coefficient and Wavelengths of Sn-Tin Samples

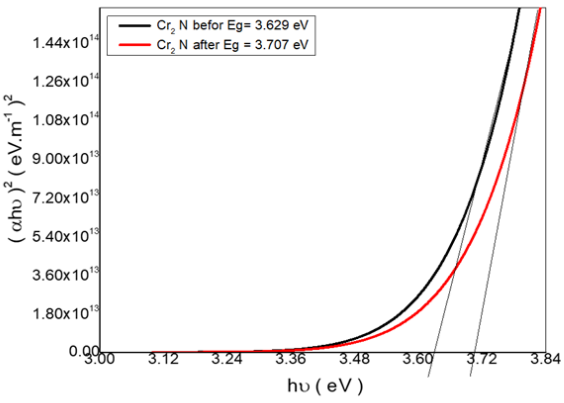

Figure 11: Optical Energy Band Gap of Cr_2N Samples

International Journal of Scientific Engineering and Science
Volume 9, Issue 9, pp. 128-134, 2025. ISSN (Online): 2456-7361

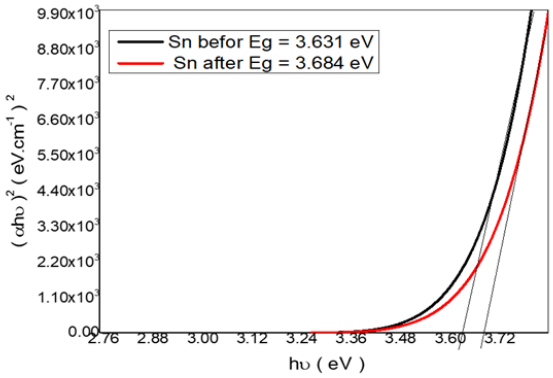

Figure 12: Optical Energy Band Gap of Sn -Tin Samples

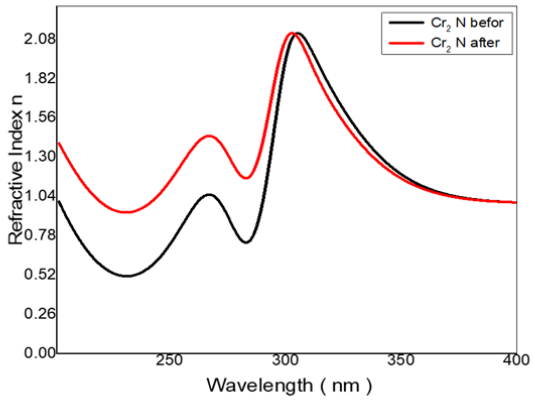

Figure 13: Relation Between Refaective Index and Wavelengths of Cr_2N Samples

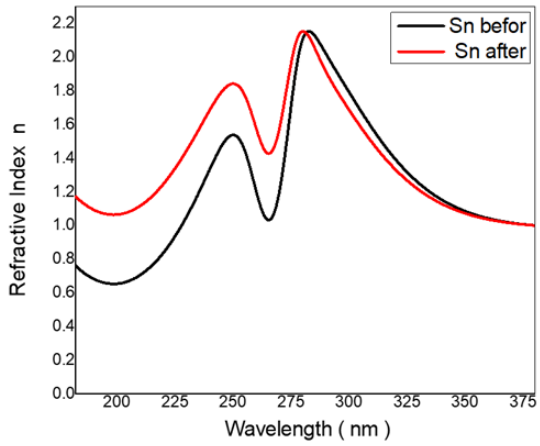

Figure 14: Relation Between Refaective Index and Wavelengths Of Sn-Tin Samples

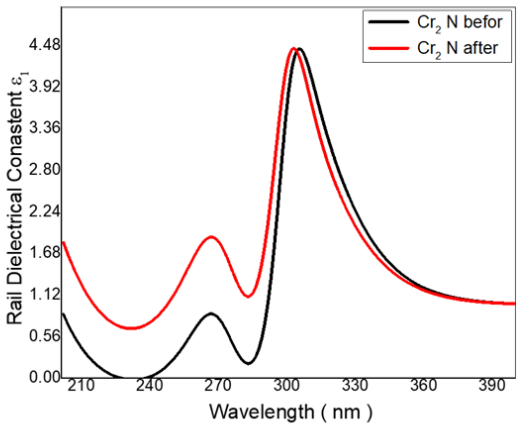

Figure 15: Relation Between Rail Dielectrical Conastant and Wavelengths of Cr_2N Samples

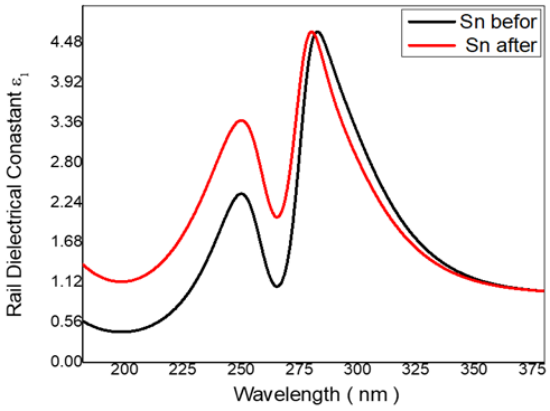

Figure 16: Relation Between Rail Dielectrical Conastant and Wavelengths of Sn-Tin Samples

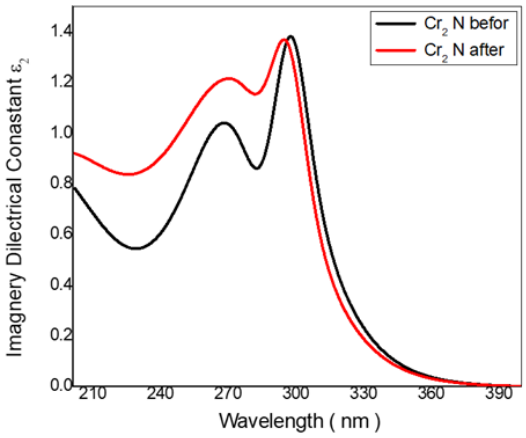

Figure 17: Relation Between Imagnery Dielectrical Conastant and Wavelengths of Cr_2N Samples

International Journal of Scientific Engineering and Science
Volume 9, Issue 9, pp. 128-134, 2025. ISSN (Online): 2456-7361

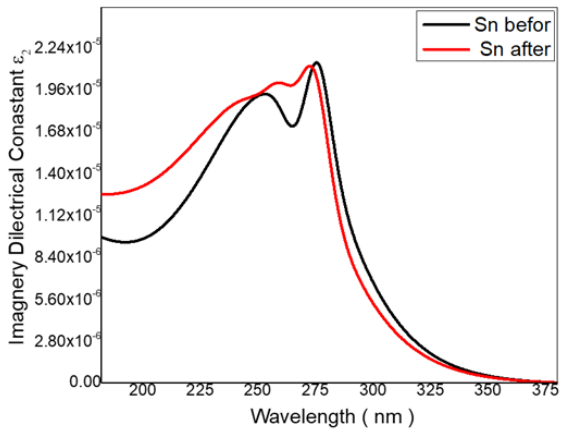

Figure 18: Relation between imagnery dielectrical conastant and wavelengths of Sn-Tin samples

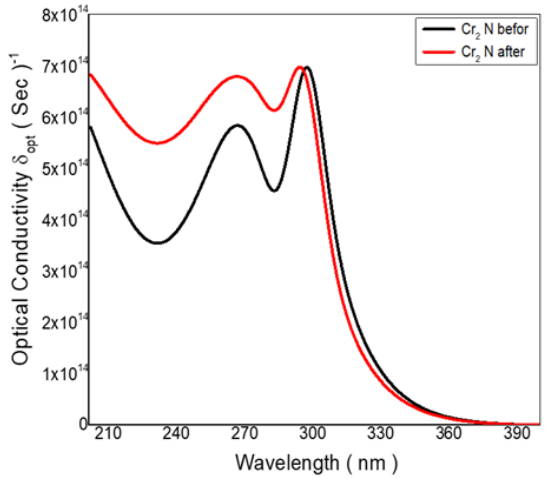

Figure 19: Relation Between Optical Conductivity and Wavelengths of Cr_2N Samples

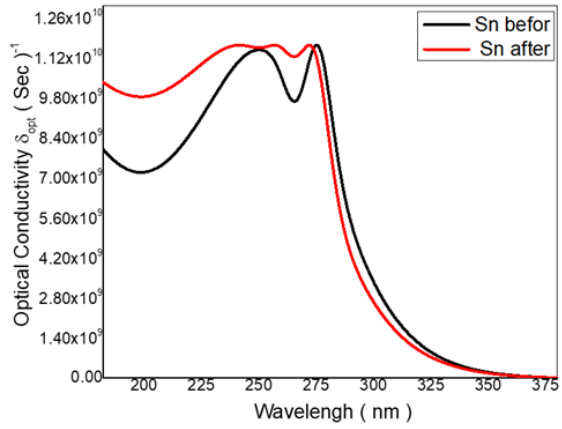

Figure 20: Relation Between Optical Conductivity and Wavelengths of Sn-Tin Samples

Conclusion and Discussion UV-VIS spectrophotometer Results of all samples

The absorbance we found the behavior of curves is the same for all (Cr_2N and Sn - Tin) samples nanoparticles studied using SPUV-26 UV/VIS 190~1100nm spectrophotometer. Show all resolute of absorbance in figure (1) for Cr_2N and figure (2) for Sn-Tin. In figure (1) shows the relation between absorbance and wavelengths for samples of Cr2N the maximal a absorption at wavelengths 230 nm corresponding photon energy 5.39 eV equal 1.0052 a.u for the samples Cr2N before grinding, but for the sample after grinding equal 0.85 a.u at the same wavelength. Also, in figure (1) show that the absorbance value decreased after grinding. And in figure (2) shows the relation between absorbance and wavelengths for Sn-Tin samples the maximal a absorption at wavelengths 195 nm corresponding photon energy 6.36 eV equal 1.0041 a.u for the samples Sn-Tin before grinding, but for the sample after grinding equal 0.83 a.u at the same wavelength. Also, in figure (2) show that the absorbance value decreased after grinding. All the absorbance curves for (Cr2N and Sn - Tin) samples nanoparticles are in ranged (202 - 400) nm.

The transmission we found the behavior of curves is the same all (Cr2N and Sn - Tin) samples nanoparticles that showing in figure (3) for Cr2N and figure (4) for Sn-Tin. In figure (3) shows the transmission for Cr2N samples, the effect of grinding on the transmission increases the transmission value after the grinding. And for figure (4) shows also the transmission for Sn-Tin samples, the effect of grinding on the transmission was increase the transmission value after grinding.

The reflection with all (Cr2N and Sn - Tin) samples nanoparticles that showing in figure (5) for Cr2N and figure (6) for Sn-Tin. In figure (5) shows that the reflection Cr2N samples was maximal value in equal 0.204 at 305 nm for Cr2N sample before grinding, but after grinding equal the same value at 300 nm. The effect of grinding on the reflection was blue shift after grinding. The reflection of Sn-Tin sample is in figure (6) shows that the maximal value in equal 0.204 at 283 nm for Sn-Tin sample before grinding, but after grinding equal the same value at 279 nm. The effect of grinding on the reflection was blue shift after grinding.

The absorption coefficient (α) of the foure prepared samples by (Cr_2N and Sn - Tin) samples nanoparticles we found from the following relation

$$\alpha = \frac{2.303xA}{t} \qquad (I)$$

where (A) is the absorbance and (t) is the optical length in the samples.

In figure (7) shows the plot of (α) with wavelength (λ) of all (Cr_2N) samples nanoparticles, which obtained that the value of $\alpha = 2.92x10^7$ cm^{-1} for Cr_2N befor grinding sample in the UV region 290 nm but for Cr_2N sample after grinding equal $2.46x10^7$ cm^{-1} at the same wavelength, this means that the transition must corresponding to direct electronic transition. Also figure (7) shows that the value of (α) for the aa samples of Cr2N decrease after grinding. And in figure(8) shows the plot of (α) with wavelength (λ) of all (Sn-Tin) samples nanoparticles, which obtained that the value of $\alpha = 4.6x10^2$ cm-1 for Sn-Tin befor grinding sample in the UV region 195 nm but for Sn-Tin sample after grinding equal $3.88x10^2$ cm-1 at

IJSES
International Journal of Scientific Engineering and Science
Volume 9, Issue 9, pp. 128-134, 2025.
ISSN (Online): 2456-7361

the same wavelength, this means that the transition must corresponding to undirect electronic transition. Also fig (8) shows that the value of (α) for the aa samples of Sn-Tin decrease after grinding.

The extinction coefficient (K) was calculated using the related

$$k = \frac{\alpha\lambda}{4\pi} \qquad (2)$$

The variation at the (K) values as a function of (λ) are shown in figure (9) for all (Cr2N) samples. Where the value of (K) at 240 nm for Cr2N sample before grinding equal 0.544 while for other sample Cr2N after grinding at the same wavelength equal 0.459. The effects of grinding on extinction coefficient (k) of all (Cr2N) samples nanoparticles was decreased after grinding. And the extinction coefficient (K) for all (Sn-Tin) samples nanoparticles in figure (10) obtained, where the value of (K) at 210 nm for Sn-Tin sample before grinding equal $7.55x10^{-6}$ while for other sample Sn-Tin after grinding at the same wavelength equal $6.32x10^{-6}$. The effects of grinding on Extinction coefficient (k) of all (Sn-Tin) samples nanoparticles was decreased after grinding.

The optical energy gap (E_g) has been calculated by the relation

$$(\alpha h\upsilon)^2 = C(h\upsilon - Eg) \qquad (3)$$

where (C) is constant.

In figure (11) the value of (E_g) of Cr2N sample before grinding equal 3.629 eV while for other sample Cr2N after grinding equal 3.707 eV.The value of (Eg) was increased from eV 3.629 eV to 3.707. The increasing of (Eg) related to grinding the samples. And in the figure (12) the value of (E_g) of all (Sn-Tin) samples nanoparticles,the energy band gap value of Sn-Tin sample before grinding equal 3.631 eV while for other sample Cr2N after grinding equal 3.684 eV. The value of(E_g) was increased from 3.63 eV to 3.684 eV. The increasing of (E_g) related to grinding the samples.

The refractive index (n) is the ratio between the speed of light in vacuum (c) to its velocity in the medium(v). The value of n was calculated from the equation

$$n = \left[\left(\frac{(1+R)}{(1-R)}\right)^2 - (1+k^2)\right]^{\frac{1}{2}} + \frac{(1+R)}{(1-R)} \qquad (4)$$

Where (R) is the reflectivity.

The variation of (n) vs (λ) for all samples nanoparticles is shown in figure (13)for Cr2N samples and figure (14) for Sn-Tin samples. Figure (4.24) Showed refractive index of all Cr2N samples. which was the maximum value of (n) is 2.135 for all Cr2N samples at 305 nm for the sample before grinding, and the same value of after grinding at 300 nm. In figure (14) Showed refractive index (n) of all Sn-Tin samples spectra, which the maximum value of (n) is 2.157 for all Sn-Tin samples at 283 nm for the sample before grinding ,and the same value of after grinding at 279 nm.

Figure (15) and figure (16) shows the variation of the real dielectric constant (ε_1) with wavelength of all samples was treetetment by (Cr_2N and Sn - Tin) nanoparticles , which calculated from the relation

$$\varepsilon_1 = n^2 - k^2 \qquad (5)$$

Where the real the dielectric (ε_1) is the normal dielectric constant.

From figure (17) the variation of (ε_1) for Cr_2N samples are follow the refractive index, where at ranged (300 to 305) nm for all samples of Cr_2N samples, where the absorption of the samples at these wavelength is small, but the polarization was increase. The maximum value of (ε_1) equal 4.412 for all Cr_2N samples at 305 nm for the sample befor grinding, will after grinding the same value at 300 nm. And for figure (18) the variation of (ε_1) for Sn-Tin samples are follow the refractive index to, where at ranged (283 to 279) nm for all samples of Sn-Tin amples, where the absorption of the samples at these wavelength is small, but the polarization was increase. The maximum value of (ε_1) equal 4.617 for all Sn-Tin samples at 283 nm for the sample befor grinding, will after grinding the same value at 279 nm.

The imaginary dielectric constant (ε_2) vs (λ) was shown in figure (19) for Cr_2N samples and figure (20) this value calculated from the relation

$$\varepsilon_2 = 2nK \qquad (6)$$

The imaginary dielectric constant (ε_2) equale 1.382 at 299 nm for Cr2N samples befor grinding, will after grinding the equal 1.371 at 293 nm. The effect of treetetment on the sample (ε_2) was blue shefte after grinding, these behavior may by related to the different absorption mechanism for free carriers. Also the imaginary dielectric constant (ε_2) equale $2.146x10^{-5}$ at 276 nm for Sn-Tin samples befor grinding, will after grinding the equal $2.116x10^{-5}$ at 273 nm. The effect of treetetment on the sample (ε_2) was blue shefte after grinding ,these behavior may by related to the different absorption mechanism forfree carriers.

The optical conductivity is a measure of frequency response of material when irradiated with light which is determined using the following relation,

$$\delta_{opt} = \frac{\alpha nc}{4\pi} \qquad (7)$$

Where (c) is the light.

The high magnitude of optical conductivity ($6.987\ x10^{14}$ sec^{-1}) at 299 nm confirms the presence of very high photo-response of the all samples prepared for Cr_2N sample befor grinding and the same value at 295 nm for the Cr_2N sample after grinding. The increased of optical conductivity at high photonenergies is due to the high absorbance of all Cr_2N samples form and may be due to electron excitation by photon energy. And high magnitude of optical conductivity ($1.164\ x10^{10}$ sec^{-1}) at 272 nm confirms the presence of very high photo-response of the all samples prepared for Sn-Tin sample befor grinding and the same value at 275 nm for the Sn-Tin sample after grinding. The increased of optical conductivity at high photonenergies is due to the high absorbance of all samples form and may be due to electron excitation by photon energy.

REFERENCES

1 Robert Odette, G.; Cunningham, N.J.; Stan, T.; Ershadul Alam, M.; de Carlan, Y. Nano-Oxide Dispersion-Strengthened Steels. In *Structural Alloys for Nuclear Energy Applications*; Robert Odette, G., Zinkle, S.J., Eds.; Elsevier: Amsterdam, The Netherlands, 2019; pp. 529–583. [Google Scholar]

2 Glasson, D.R.; Jayaweera, S.A.A. Formation and Reactivity of Nitrides I. Review and Introduction. *J. Appl. Chem.* 1968, *18*, 65–77. [Google Scholar] [CrossRef]

3 Eklund, P.; Kerdsongpanya, S.; Alling, B. Transition-Metal-Nitride-Based Thin Films as Novel Energy Harvesting Materials. *J Mater. Chem. C Mater.* 2016, *4*, 3905–3914. [Google Scholar] [CrossRef] [Green Version]

4 Barata, A.; Cunha, L.; Moura, C. Characterisation of Chromium Nitride Films Produced by PVD Techniques. *Thin Solid Film.* 2001, *398–399*, 501–506. [Google Scholar] [CrossRef] [Green Version]
5 Sanjinés, R.; Hones, P.; Lévy, F. Hexagonal Nitride Coatings: Electronic and Mechanical Properties of V2N, Cr2N and δ-MoN. *Thin Solid Film.* 1998, *332*, 225–229. [Google Scholar] [CrossRef]
6 Lin, J.; Moore, J.J.; Sproul, W.D.; Mishra, B.; Wu, Z.; Wang, J. The Structure and Properties of Chromium Nitride Coatings Deposited Using Dc, Pulsed Dc and Modulated Pulse Power Magnetron Sputtering. *Surf. Coat Technol.* 2010, *204*, 2230–2239. [Google Scholar] [CrossRef]
7 Ahn, S.H.; Choi, Y.S.; Kim, J.G.; Han, J.G. A Study on Corrosion Resistance Characteristics of PVD Cr-N Coated Steels by Electrochemical Method. *Surf. Coat Technol.* 2002, *150*, 319–326. [Google Scholar] [CrossRef]
8 Liu, C.; Bi, Q.; Matthews, A. EIS Comparison on Corrosion Performance of PVD TiN and CrN Coated Mild Steel in 0.5 N NaCl Aqueous Solution. *Corros. Sci.* 2001, *43*, 1953–1961. [Google Scholar] [CrossRef]
9 Zhou, L.; Körmann, F.; Holec, D.; Bartosik, M.; Grabowski, B.; Neugebauer, J.; Mayrhofer, P.H. Structural Stability and Thermodynamics of CrN Magnetic Phases from Ab Initio Calculations and Experiment. *Phys. Rev. B Condens. Matter Mater. Phys.* 2014, *90*, 184102. [Google Scholar] [CrossRef] [Green Version]
10 Abdallah, B.; Kakhia, M.; Alssadat, W.; Zetoun, W. Study of Power Effect on Structural, Mechanical Properties and Corrosion Behavior of CrN Thin Films Deposited by Magnetron Sputtering. *Prot. Met. Phys. Chem. Surf.* 2021, *57*, 80–87. [Google Scholar] [CrossRef]